



OPEN

SUBJECT AREAS:
FUEL CELLS
ELECTROCATALYSISReceived
9 July 2014Accepted
2 October 2014Published
22 October 2014Correspondence and
requests for materials
should be addressed to
D.X. (xiaodan@scu.
edu.cn)

Enhanced Electrocatalytic Performance for Oxygen Reduction via Active Interfaces of Layer-By-Layered Titanium Nitride/Titanium Carbonitride Structures

Zhaoyu Jin¹, Panpan Li^{1,2} & Dan Xiao¹¹Key Laboratory of Green Chemistry and Technology, Ministry of education, College of Chemistry, Sichuan University, Chengdu 610064, P. R. China, ²College of Architecture and Environment, Sichuan University, Chengdu 610065, P. R. China.

Cathode materials always limit the performance of fuel cells while the commercial platinum-based catalysts hardly meet the requirements of low cost, durable and stable. Here a non-precious metal oxygen reduction reaction (ORR) electrocatalyst based on titanium nitride/titanium carbonitride hierarchical structures (TNTCNHS) is demonstrated as high activity as Pt/C. In alkaline condition, tuning interface/mass ratio of TiN/TiCN, we observed the onset potential of ~ 0.93 V vs. RHE and a limit diffusion current density of ~ 5.1 mA cm⁻² (at a rotating speed of 1600 rpm) on TNTCNHS with a relative low catalyst loading of ~ 0.1 mg cm⁻². The kinetic current, durability and tolerance to crossover effect studies reveal even more efficient than carbon-supported platinum. The architecture fabrication for such electrocatalyst is easy to realize in industrial-scale facilities, for the use of chemical vapor deposition (CVD) technique could support a huge area production (more than 10000 cm² for one pot) to satisfy the enormous market requirements in the future.

Polymer electrolyte fuel cells (PEFCs) with high energy yield and low environmental impact has been focused by a huge number of researches, which are considered to be the most promising energy conversion technologies available today¹. The cathode oxygen reduction reaction (ORR) of PEFCs acts as a critical role in controlling the performance^{2,3}, for being always six or more times of magnitude slower than the anode hydrogen oxidation reaction⁴. Additionally, the ORR is also important in metal-air batteries⁵⁻⁷, water electrolysis, corrosion and so on^{8,9}. Traditional cathode materials of fuel cells are used platinum as an active ORR catalyst, with the high price of this precious metal having a limitation on its economic usefulness. Apart from the high cost, Pt-based catalysts also suffer from limited durability¹⁰⁻¹² and carbon monoxide, methanol or other small organic molecules deactivation^{3,13,14}. Therefore, Pt replacement candidates that attracts the most attention have been reported widely recently including metal oxides¹⁵⁻¹⁸, carbides^{19,20}, nitrides^{21,22}, chalcogenides^{23,24} and nitrogen-doped carbons^{3,7,25,26}. However, rare materials can do satisfy the requirement of activity and stability for ORR in PEFC condition referring to platinum and to realize manufacture in large quantities is also a problem in practical industry.

Titanium nitride (TiN) leads the electrocatalytic activity among various metal nitrides since its more active sites, stronger adsorption ability and much cheaper than Pt^{21,27}. According to the market price, TiN reagent is $\sim \$ 1.0$ per gram compared with $\sim \$ 95$ per gram of Pt/C reagent, while the industrialized manufacture of TiN would further cut down the cost even less than $\$ 0.1$ per gram but industrialized Pt hardly decrease its spending so much. Nevertheless, the reported TiN nanostructures with inferior ORR performance in accordance with Pt-based catalysts haven't reach the height for catalysis in the cathode reaction of PEFCs yet, even though the small enough particle size and the use of ideal supports like carbon black, carbon nanotube or graphene. Because the injected electrons to TiN would be difficult to finish the O-O bond dissociated easily, which bring about two-electron oxygen reduction process and the generation of undesirable H₂O₂^{21,22,28,29}. In general, transition metal nitride/carbide ought to play a crucial role in the practical applications of optical, electronic, magnetic and catalytic area, contrast with oxides and carbon materials, attributing to the high electrical conductivity, hardness and durability^{30,31}. Thus, to solve the issue fundamentally, the architecture of electrocatalyst should be designed to

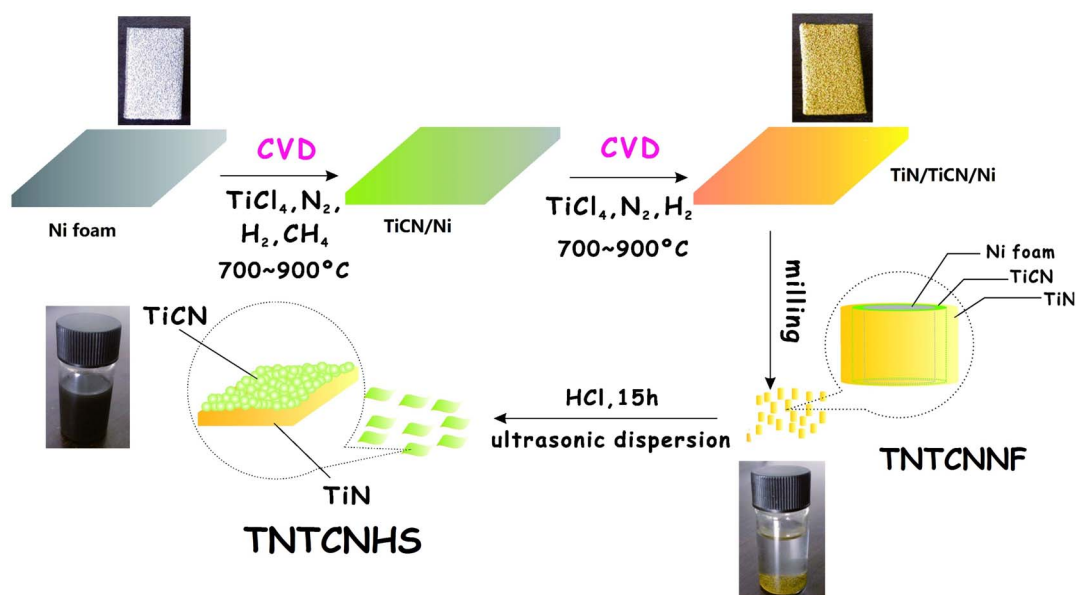


Figure 1 | Schematic diagram of the synthesis of TNTCNHS catalysts.

improve the adsorption mode on nitride so that the electron could be injected more effectively from the catalyst to oxygen.

Herein we use a facile strategy of chemical vapor deposition (CVD) to grow TiCN and TiN thin films in two-step on the nickel foam template. After milling, the Ni is removed by acid and a hierarchical TiN/TiCN structure is obtained. In addition, the electrocatalytic activity for oxygen reduction reaction is studied and evaluated. The catalyst displays a highly improved activity compared with TiN and TiCN in alkaline environment, which is found to be even more efficient than commercial 20% wt Pt/C, as well as also better durability and tolerance to methanol in the cathode reaction of PEFCs.

Results

The TNTCNHS were prepared via CVD process and the removal of template as illustrated in Figure 1. Above all, Ni foam was firstly coated on TiCN thin films via CVD, as soon as TiN thin films were deposited on TiCN to obtain TiN/TiCN/Ni thin films (TNTCNHF).

As the photographs show, the Ni foam with yellow deposits became fragile so that it could be milled to uniform powder. Finally, hydrochloric acid was employed to dissolve the Ni template and TNTCNHS was obtained under ultrasonic wave. The color of the catalyst after dried had become black yellow and the dispersion was greatly improved in ethanol. The thickness of each layer could be easy to tune via controlling the airflow of the mixed gas and the multilayer deposits always keep uniform, dense, good crystallinity and closely integrated with the substrates³². Figure 2A and 2B are the scanning electron microscopy (SEM) images of the two sides of TNTCNHS respectively. As we see the TiN side shows ~100 nm diameter crystals array densely and smaller size TiCN nanoparticles (NPs) on the opposite displays porous structures which would supply high specific surface area for catalysis. The interface of the TiN and TiCN (TNTCNHS-1) is also observed in Figure 2C (TNTCNHS-2 with thicker layers is shown in the inset). The compact structures of two compositions are likely to make them score high in electron transfer

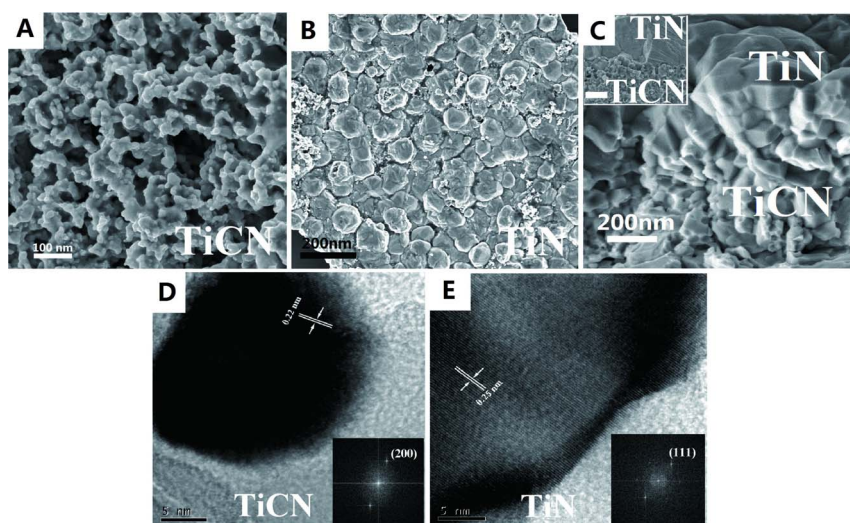


Figure 2 | SEM images of (A) TiCN side, (B) TiN side and (C) the interface of TiN and TiCN (TNTCNHS-1) and the inset shows the interface of TNTCNHS-2 (The scale bar is 200 nm). TEM images and corresponding FFT patterns of (D) TiCN and (E) TiN crystal on TNTCNHS.



and stability. The corresponding transmission electron microscopy (TEM) images and fast Fourier transform (FFT) patterns are in Figure 2D and 2E, which indicate the (200) of TiCN and (111) of TiN. Here we put forward a facile method to construct double-layer structures by using chemical vapor deposition.

X-ray diffraction (XRD) pattern of the TNTCNHS is shown in Figure S1A which indicates our prepared catalyst is TiN/TiCN with good crystallization. However, the unit cell parameters of titanium nitride and titanium carbonitride are too closed, thus it could not be confirmed both of them two exist in the catalyst. Therefore, X-ray photoelectron spectroscopy (XPS) is utilized to determine the elements and chemical bonds. Figure S1B demonstrates a XPS survey and high resolution spectrums of Ti 2p, N 1s and C 1s in TNTCNHS with the element carbon as internal standard (B.E. = 284.6 eV). Obviously, the binding energy (B.E.) of Ti-N could be examined at Ti 2p_{3/2} (B.E. = 456.3 eV), Ti 2p_{1/2} (B.E. = 461.2, 464.0 eV) and N 1s (B.E. = 397.3 eV), while the Ti-C and C-N bond are confirmed by the Ti 2p_{3/2} (B.E. = 455.1 eV), C 1s (B.E. = 281.5 eV and 287.8 eV), and N 1s (B.E. = 295.8 eV).

The ORR activity of various catalysts containing TNTCNHS, TiN/TiCN/Ni thin film (TNTCNTF), broken hierarchical structure of blending TiN/TiCN nanocomposites (TNTCNNC, see the synthesis method in Supporting Information and SEM images in Figure S2), commercial TiN nanoparticles (TNNP), TiCN nanoparticles (TCNNP) and Pt/C (20 wt%) are shown in Figure 3 and Figure S3–S8. Linear sweep voltammetry (LSV) with rotating disk electrode (RDE) studies of TNTCNHS was conducted at room temperature and in 0.1 M KOH electrolyte. Figure 3A illustrates the polarization curves of TNTCNHS-1 at different rotating speed in O₂-saturated alkaline solution, indicating that the onset potential is ~0.93 V vs.

RHE and the limiting diffusion current density increases with increasing rotation rate. The corresponding Koutecky-Levich (K-L) plots are shown in Figure 3B from 0.3 V to 0.6 V, and the average number of electrons transferred (*n*) during the ORR are calculated to be ~4.0 for TiN/TiCN hierarchical structures. TNTCNHS-2 which owns smaller interface/mass ratio than TNTCNHS-1 is also revealed as a good ORR catalysts and the corresponding linear sweep voltammetric curves for RDE testing is displayed in Figure 3C. The average of transfer electron number is ~3.96 calculated from its K-L plots (Figure S3). The ORR polarization curves and K-L plots of other catalysts are also determined exhibited in Supporting Information. For more detail discussion, Tafel plots of the steady-state polarization curves were carried out to investigate oxygen reduction reaction rate. The corresponding Tafel slopes of TNTCNHS-1, TNTCNHS-2 and Pt/C are shown in Figure 3D, which present closed values indicating that TNTCNHS catalyst will lead to a fast increment of reaction rate with increasing overpotential as well as platinum³³.

Summarized LSV curves for TNNP, TCNNP, TNTCNTF, TNTCNNC, Pt/C and TNTCNHS are shown in Figure 4A where our prepared TiN/TiCN hierarchical structures reveal a closed onset potential ($\Delta E_{\text{onset}} = \sim 30$ mV) and half-wave potential ($\Delta E_{1/2} = \sim 38$ mV) to Pt/C, even the current density has overtaken platinum's obviously at the more negative potential than 0.7 V. Electrochemical impedance spectroscopy was also utilized to test the electron transfer resistance (*R*_{et}) of TNTCNHS, TNNP and TCNNP at 0.8 V where a mixed kinetic-diffusion control region for ORR existed (Figure S9). The Nyquist plots demonstrated the hierarchical structures show smaller *R*_{et} than single components of TiN and TiCN. Therefore, the TNTCNHS is the most effective catalysts in shuttling charges

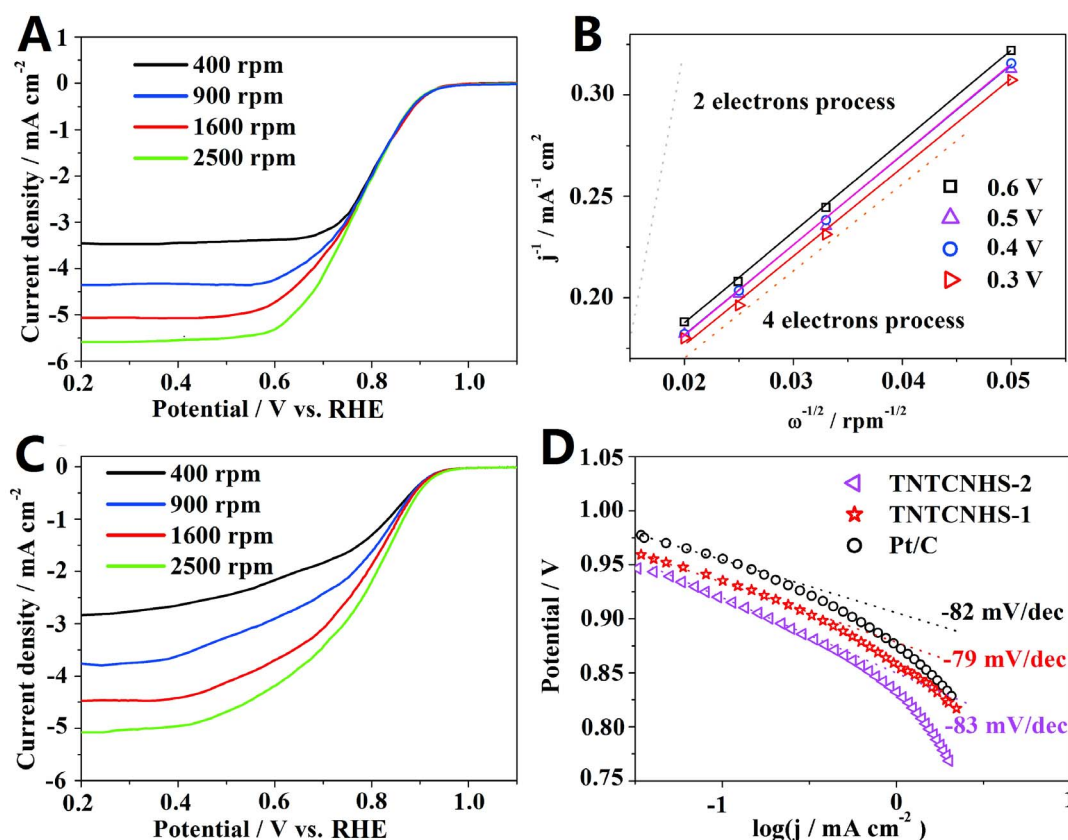


Figure 3 | (A) Polarization curves of TNTCNHS-1 at rotating speed of 400–2500 rpm in O₂-saturated 0.1 M KOH. (B) The corresponding K-L plots of TNTCNHS at 0.6 V–0.3 V. (C) Polarization curves of TNTCNHS-2 in O₂-saturated 0.1 M KOH. (D) Corresponding Tafel plots of TNTCNHS-1, TNTCNHS-2 and commercial Pt/C. The catalysts loading are all kept at ~0.1 mg cm⁻².

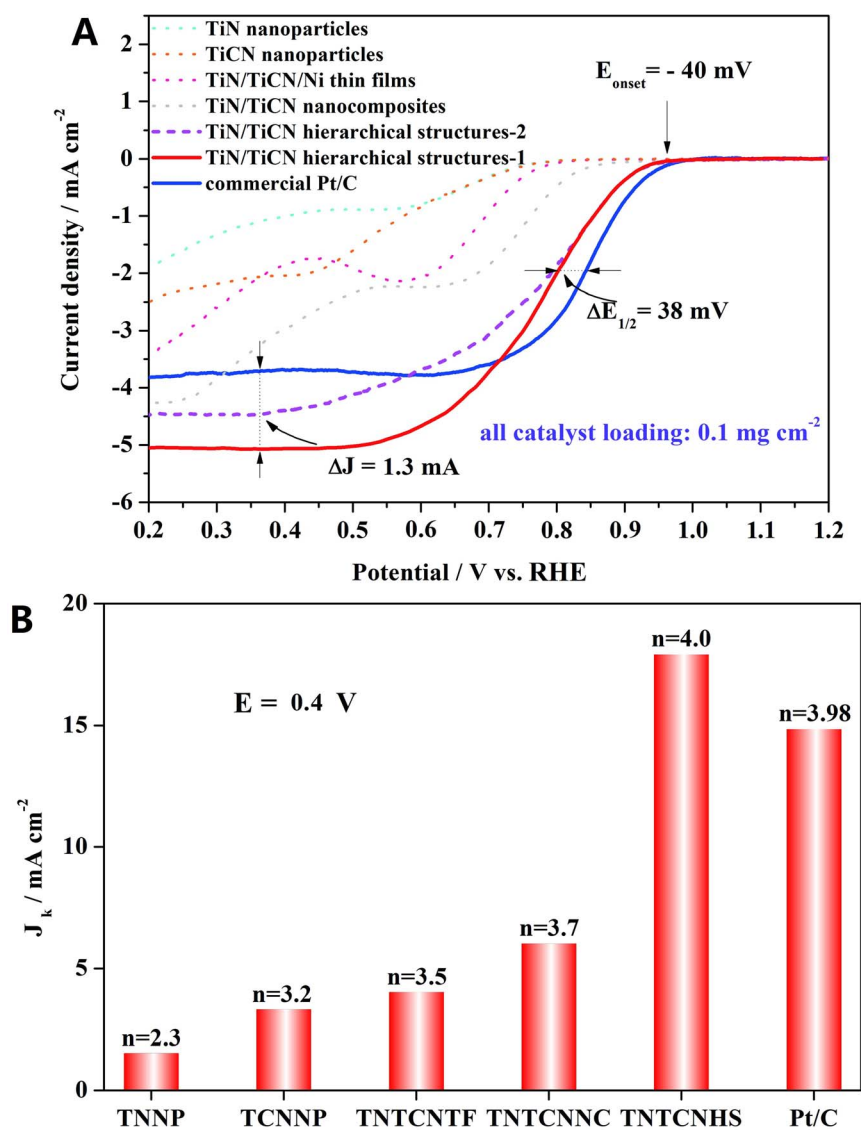


Figure 4 | (A) Compared polarization curves of TNNP, TCNNP, TNTCNTF, TNTCNNC, TNTCNHS and Pt/C at 1600 rpm. The catalyst loadings for RDE are all kept at 0.1 mg cm^{-2} . (B) Bar diagram of the calculated kinetic current and electron transfer number.

from electrode to solution, and the catalytic activity for ORR can be remarkably promoted³⁴. The kinetic current density of various catalysts was also calculated to compare the activity for ORR, which is considered as a convincing parameter in electrochemical reaction process. Figure 4B demonstrates the comparisons of kinetic current density and electron transfer number at 0.4 V vs. RHE, where our prepared TNTCNHS displays a great enhancement (17.8 mA cm^{-2}) refer to TNNP (1.5 mA cm^{-2}) and TCNNP (3.3 mA cm^{-2}) as well as even obviously superior to Pt/C (14.8 mA cm^{-2}).

The durability of the TNTCNHS and commercial Pt/C catalysts was also evaluated by using a chronoamperometric method at 0.7 V (Figure 5A). The TNTCNHS shows higher stability (holds $\sim 95\%$ current density) than that of Pt/C (holds $\sim 75\%$ current density) with only a little decline in its activity during a 35000 s testing period. Moreover, Methanol tolerance is an important requirement for cathode materials in direct methanol fuel cells (DMFC) and also a remarkable shortcoming of Pt-based catalysts. The inset figure shows almost no effect on the oxygen reduction activity of TNTCNHS although 1 M methanol was added to the electrolyte, while the current density of Pt/C dropped more than 15% immediately.

The single cell testing was carried out in this study shown in Figure 5B. A $\text{H}_2 - \text{O}_2$ alkaline fuel cell (AFC) was constructed to

compare our prepared TNTCNHS and commercial Pt/C for cathode materials. As we see, the I-V curves reveal closed performance of two catalysts where the open circuit potential of TNTCNHS (0.96 V) has overtaken platinum (0.92 V) and the maximum power density are both $\sim 100 \text{ mW cm}^{-2}$ for Pt/C and $\sim 82 \text{ mW cm}^{-2}$ for TNTCNHS-1. Considering such excellent performance as AFC cathode catalyst, we believe it would be a promising non-precious material for the electrocatalysis of oxygen reduction reaction to take place Pt-based catalysts in practical applications.

Discussion

To investigate the improved ORR performance TNTCNHS-1 referring to TNTCNHS-2, we took SEM images of the cross-view (Figure 6A). The thickness of two catalysts are observed clearly which proves TNTCNHS-1 owns thinner TiN and TiCN layers ($2 \mu\text{m}$ vs. $8 \mu\text{m}$). While the mass loadings of the catalysts on the disk electrode are kept identical, it is obvious the hierarchical structures with thinner layers would expose more surface and interface. To find electrochemical active surface area (EASA), we measured the non-faradic charged - discharged current associated with electrochemical double layer capacity (C_{dl}) upon cyclic voltammetry^{35,36}. Figure S10 shows larger C_{dl} of TNTCNHS-1 than TNTCNHS-2 indicating larger

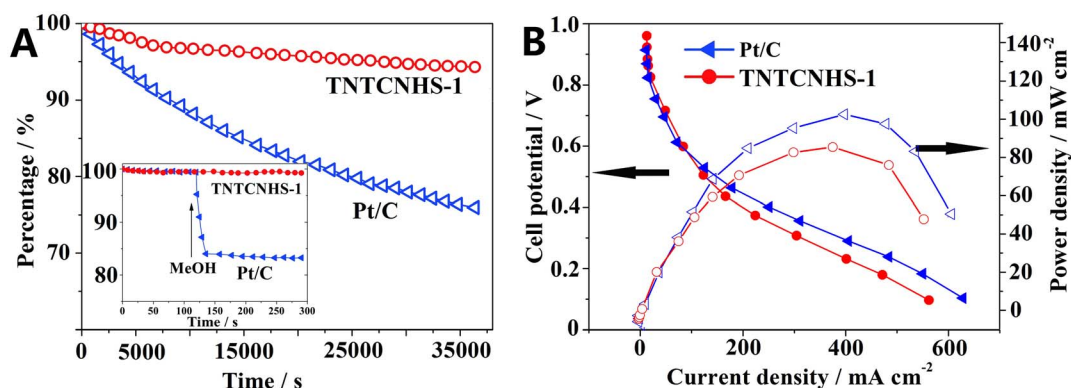


Figure 5 | (A) The chronoamperometric responses for the ORR on the TNTCNHS-1 and commercial Pt/C catalyst at 0.7 V. Inset shows the current response with 1 M methanol added. Rotating speed: 400 rpm. (B) Single cell testing of the TNTCNHS-1 and commercial Pt/C as cathode catalysts with a loading of 4 mg cm⁻² and 2 mg cm⁻², respectively. Anode catalysts are both platinum on carbon ($m_{\text{Pt}} = \sim 0.4 \text{ mg cm}^{-2}$).

EASA. The high specific surface area of TiN or TiCN haven't ensured such superior activity that TNTCNHS exhibits, because neither TiN nor TiCN NPs can be as efficient electrocatalysts for ORR (see in Figure S4 and S5). By contrasted with TNTCNHC (interface is destroyed), the interface between TiN and TiCN layers probably makes the contribution to ORR (a scheme is shown in Figure 6B). TNTCNHS-1 holds almost four times larger area of the interface than TNTCNHS-2, which brings the enhancement of $\Delta J = \sim 0.5 \text{ mA cm}^{-2}$ at 0.4 V. A deep insight about the active interfaces in this study is carried out by the calculation in the following of the discussion.

It seems to understand why the hierarchical structures of TiN/TiCN have such a high activity is important; XPS of the sample was studied in Figure S11, which was collected after going through the process of oxygen reduction. Strong binding energy of Ti-O was examined at the high resolution spectrums of Ti 2p and O 1s (458.0 eV, 531.2 eV and 529.5 eV). Thus, the titanium atoms in TiN and TiCN crystals are probably considered as the active sites in electrocatalytic reaction. In a typical ORR, firstly, oxygen molecules are adsorbed at the surface of the catalyst via Ti-O bond and then O-O bond is dissociated for further reduction to OH⁻ in alk-

aline solution. If the O-O bond is not dissociated, undesirable HO₂⁻ is obtained²⁷. The ORR performance, therefore, is majorly depended on two crucial steps that one is the sites for oxygen chemisorption and the other is the electron injection from catalyst to electroactive substance. The traditional adsorption is single oxygen atom binding with the active site atom on the surface of catalyst via chemical bond such as the path I and path II in the model of Figure 7A. However, this mode requires the active site atom has enough high positive charge density to restrain free molecular oxygen. On the other aspect, the O-O bond is stable so that it is hard to dissociate with low energy supplied. Hence, we proposed another adsorption mode at our high ORR activity catalyst of TNTCNHS that the two oxygen atoms in one molecule could be reacted with Ti atoms from double-side at the interface of the TiN and TiCN simultaneously (as the path III). The TEM image of the interface between TiN and TiCN is fortunately recorded which shows the distance ranged from $\sim 0.2 \text{ nm}$ to 1 nm in Figure 7B. As we know, the diameter of oxygen molecule is $\sim 0.3 \text{ nm}$ so that it would be reasonable for the proposed adsorption mode. To confirm the observed interface is indeed between the TiN and TiCN, we compare the FFT patterns of the two particles in Figure S12, which are fitting well with the results in Figure 2D and 2E,

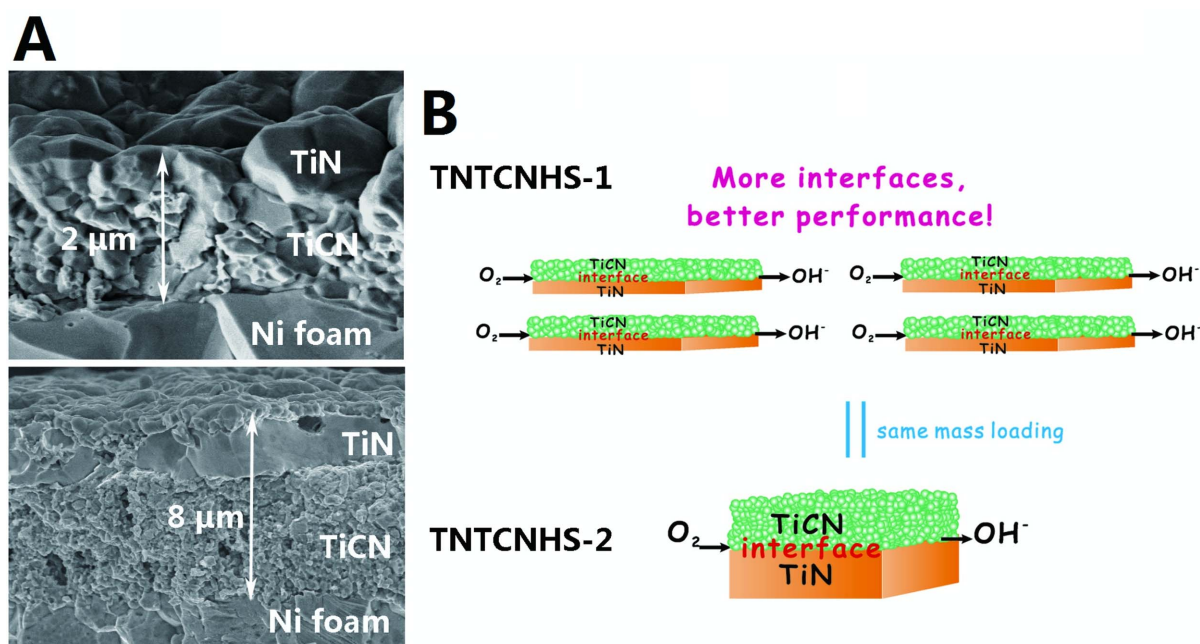


Figure 6 | (A) SEM images of the cross-view of TNTCNHS-1 and TNTCNHS-2 before Ni template removed. (B) Schematic the active interfaces of TNTCNHS.

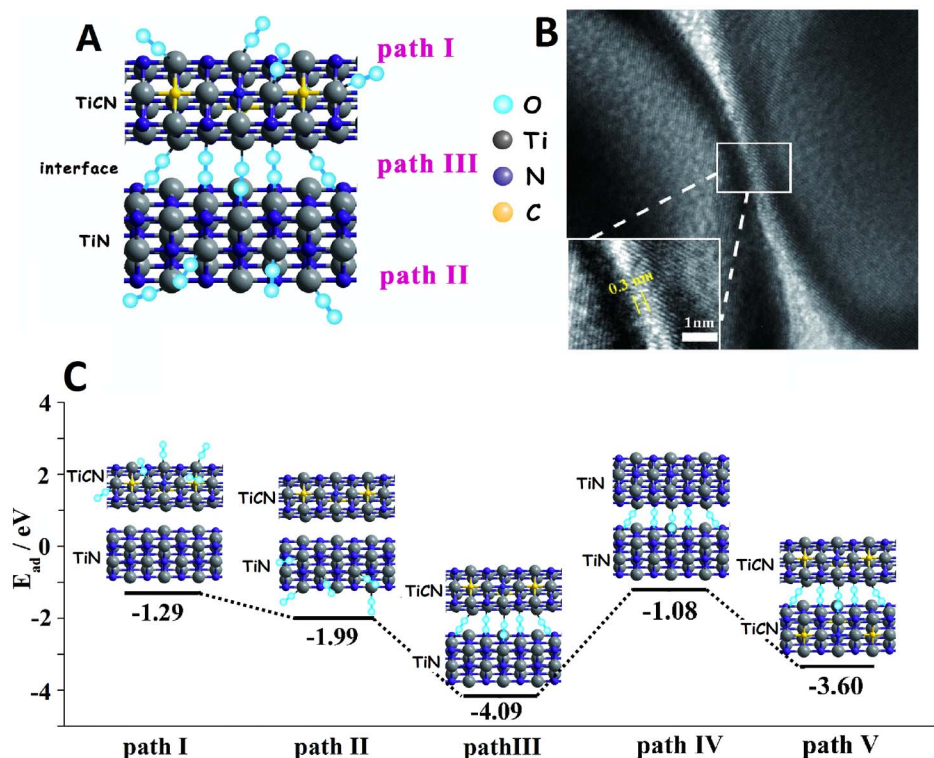


Figure 7 | (A) A model for the three adsorption paths of O_2 on TNTCNHS. (B) The calculated adsorption energies of three possible adsorption paths on TNTCNHS and other two paths on TiN/TiN and TiCN/TiCN hierarchical structures (path IV and path V).

indicating both TiN and TiCN are presence. Another two modes for oxygen adsorption which were the TiN - O_2 - TiN and TiCN - O_2 - TiCN systems (path IV and path V) were also considered for the situations of TNNP or TCNNP catalyst, although most of the particles were separated from a related long distance so that the double-side adsorption almost couldn't take place. The adsorption energies (E_{ad}) of the five modes were also obtained by density functional theory (DFT) calculations (Figure 7C, see the Supporting Information for the molecular models of Figure S13). Our proposal path III displays lower E_{ad} (-4.09 eV) than other four indicating that this adsorption mode could be more efficient and easier for Ti-O bonds generation. In addition, the porous structure of the TNTCNHS also provides a number of tunnels for the transport of O_2 and electrolyte to the interface. The charge density of the Ti atoms in TiN and TiCN are also calculated, which is 0.74 and 0.72 respectively. The gap of the electric charge at the two sides of active site could be positive for the dissociation of the adsorbed electronegative oxygen molecule because the electrons of O-O bond would sides of the catalyst to O_2 . As for TNNP and TCNNP, most adsorptions take place on single oxygen atom (path I and path II, $E_{ad} = -1.29$ and -1.99 eV respectively) and only a few O_2 might be absorbed by two Ti atoms (path IV and path V, $E_{ad} = -1.08$ and -3.60 eV respectively). Moreover, these paths couldn't weaken the stability of O-O bond so that there aren't satisfied activities, concerning the onset potential, limit diffusion current and transfer electron number observed from Figure S4 and Figure S5. Because of limited region for the double-side adsorption, most of space is remained to transport the electrolyte, reactants and products between the external solution and the interface. Figure S14 reveals a schematic process for the entrance and exit of OH^- and O_2 . Further study has started to investigate the interface via more sound approach and to extend this active specific area is also needed in the following work.

In summary, we construct TiN/TiCN hierarchical structures via layer-by-layered CVD method. After removal of template, the obtained powder (TNTCNHS-1) displays an enhanced ORR activity

in alkaline electrolyte, which exhibits a low onset potential of 0.93 V, high limit diffused current density of 5.1 mA cm^{-2} at 1600 rpm and smaller Tafel slope of 79 mV dec^{-1} . The stability and single cell testing also reveal the more excellent performance of TNTCNHS-1 compared with commercial Pt/C. Moreover, the interface between TiN and TiCN layers is considered as an active region for oxygen adsorption. Such high performance cathode catalyst for AFC provides three adsorption modes for ORR which displays strong oxygen utilization. Further, TiN and TiCN also have good electric conductivity, excellent wear and high temperature resistance³⁰⁻³², so it would be employed at both ambient and extreme conditions. Chemical vapor deposition have been a mature and large-area productive technique for the relatively low-cost manufacture with industrial-scale facilities, as well as the strategy for the construction of hierarchical structures is facile, rapid, cheap and universal. Thus, to build the active interfaces on double-layered architecture like TNTCNHS might enable more electrocatalysts to achieve a new class of activity that they can rarely reached in traditional constructions.

Methods

TiCN film was firstly coated on Ni foams ($2 \times 4 \text{ cm}$) via chemical vapor deposition. In a typical CVD process, $TiCl_4$ (Kermel Chemical Reagent Company, China) was chosen as a Ti source with N_2 , CH_4 and H_2 ($TiCl_4: N_2: CH_4: H_2 = 2:1:1:100$, v/v) to pass into a CTI-C280A MT-CVD device system ($\Phi 240 \times H500$, Chengdu Tool Research Institute Co. Ltd, China) at $700 \sim 900^\circ\text{C}$ for 1 h. About 1200 pieces of Ni foam with total surface area of more than 10000 cm^2 can be deposited simultaneously. And then TiN film was also coated on the same Ni foams in a similar procedure with $TiCl_4$, N_2 and H_2 ($1:1:25$, v/v) for ~ 1 h. After cooled to room temperature, Ni foam coated with TiN/TiCN films was carried out and washed by distilled water and ethanol. Afterwards, the coated Ni was milled to powder and the TiN/TiCN thin films (TNTCNHF) were obtained. Then Ni foam template was removed by 2 M hydrochloric acid at 50°C for 15 h followed with ultrasonic dispersion to homogenous. Finally, the TiN/TiCN hierarchical structures catalyst was filtered, rinsed by distilled water and ethanol for three times and dried at 60°C in vacuum. The thickness of the TiCN and TiN layers can be adjusted by controlling the flow rate (v) of the hydrogen ($v_{TNTCNHS-1} \sim 40\%$, $v_{TNTCNHS-2} \sim 800 \text{ cm}^3 \text{ min}^{-1}$) We also prepared the broken hierarchical structure of blending TiN/TiCN nanocomposites (TNTCNHC) with the same CVD process but coating on a smooth nickel plate. Next the Ni plate was directly immersed into 4 M hydrochloric acid at 60°C for 24 h without need of milling to



powder. After ultrasonic dispersion to homogenous, the TNTCNCC was filtered, wash and dried as above described.

- Wu, G., More, K. L., Johnston, C. M. & Zelenay, P. High-Performance Electrocatalysts for Oxygen Reduction Derived from Polyaniline, Iron, and Cobalt. *Science* **332**, 443–447 (2011).
- Steele, B. C. H. & Heinzel, A. Materials for fuel-cell technologies. *Nature* **414**, 345–352 (2001).
- Gong, K. P., Du, F., Xia, Z. H., Durstock, M. & Dai, L. M. Nitrogen-Doped Carbon Nanotube Arrays with High Electrochemical Activity for Oxygen Reduction. *Science* **323**, 760–764 (2009).
- Debe, M. K. Electrocatalyst approaches and challenges for automotive fuel cells. *Nature* **486**, 43–51 (2012).
- Dewi, E. L., Oyaizu, K., Nishide, H. & Tsuchida, E. Electrocatalysis for dioxygen reduction by a mu-oxo decavanadium complex in alkaline medium and its application to a cathode catalyst in air batteries. *J. Power Sources* **130**, 286–290 (2004).
- Girishkumar, G., McCloskey, B., Luntz, A. C., Swanson, S. & Wilcke, W. Lithium-Air Battery: Promise and Challenges. *J. Phys. Chem. Lett.* **1**, 2193–2203 (2010).
- Chung, H. T., Won, J. H. & Zelenay, P. Active and stable carbon nanotube/nanoparticle composite electrocatalyst for oxygen reduction. *Nat. Commun.* **4**, 1922 (2013).
- Dau, H. *et al.* The Mechanism of Water Oxidation: From Electrolysis via Homogeneous to Biological Catalysis. *Chemcatchem* **2**, 724–761 (2010).
- Tiwari, J. N. *et al.* Stable platinum nanoclusters on genomic DNA-graphene oxide with a high oxygen reduction reaction activity. *Nat. Commun.* **4** (2013).
- Stamenkovic, V. R. *et al.* Improved Oxygen Reduction Activity on Pt₃Ni(111) via Increased Surface Site Availability. *Science* **315**, 493–497 (2007).
- Peng, Z. & Yang, H. Synthesis and Oxygen Reduction Electrocatalytic Property of Pt-on-Pd Bimetallic Heterostructures. *J. Am. Chem. Soc.* **131**, 7542–7543 (2009).
- Yu, X. W. & Ye, S. Y. Recent advances in activity and durability enhancement of Pt/C catalytic cathode in PEMFC - Part II: Degradation mechanism and durability enhancement of carbon supported platinum catalyst. *J. Power Sources* **172**, 145–154 (2007).
- Winter, M. & Brodd, R. J. What are batteries, fuel cells, and supercapacitors? *Chem. Rev.* **104**, 4245–4269 (2004).
- Zhu, C. Z., Guo, S. J. & Dong, S. J. PdM (M = Pt, Au) Bimetallic Alloy Nanowires with Enhanced Electrocatalytic Activity for Electro-oxidation of Small Molecules. *Adv. Mater.* **24**, 2326–2331 (2012).
- Zhu, H. Y., Zhang, S., Huang, Y. X., Wu, L. H. & Sun, S. H. Monodisperse MxFe₃-xO₄ (M = Fe, Cu, Co, Mn) Nanoparticles and Their Electrocatalysis for Oxygen Reduction Reaction. *Nano. Lett.* **13**, 2947–2951 (2013).
- Liang, Y. Y. *et al.* Co₃O₄ nanocrystals on graphene as a synergistic catalyst for oxygen reduction reaction. *Nat. Mater.* **10**, 780–786 (2011).
- Guo, S. J., Zhang, S., Wu, L. H. & Sun, S. H. Co/CoO Nanoparticles Assembled on Graphene for Electrochemical Reduction of Oxygen. *Angew. Chem. Int. Ed.* **51**, 11770–11773 (2012).
- Cheng, F. Y. *et al.* Enhancing Electrocatalytic Oxygen Reduction on MnO₂ with Vacancies. *Angew. Chem. Int. Ed.* **52**, 2474–2477 (2013).
- Lee, K. C., Ishihara, A., Mitsushima, S., Kamiya, N. & Ota, K. I. Stability and electrocatalytic activity for oxygen reduction in WC plus Ta catalyst. *Electrochim. Acta* **49**, 3479–3485 (2004).
- Kelly, T. G. & Chen, J. G. Metal overlayer on metal carbide substrate: unique bimetallic properties for catalysis and electrocatalysis. *Chem. Soc. Rev.* **41**, 8021–8034 (2012).
- Youn, D. H. *et al.* A highly efficient transition metal nitride-based electrocatalyst for oxygen reduction reaction: TiN on a CNT-graphene hybrid support. *J. Mater. Chem. A* **1**, 8007–8015 (2013).
- Wang, Y. R. *et al.* Nano- and micro-sized TiN as the electrocatalysts for ORR in Li-air fuel cell with alkaline aqueous electrolyte. *J. Mater. Chem.* **22**, 15549–15555 (2012).
- Vante, N. A., Jaegermann, W., Tributsch, H., Honle, W. & Yvon, K. Electrocatalysis of Oxygen Reduction by Chalcogenides Containing Mixed Transition-Metal Clusters. *J. Am. Chem. Soc.* **109**, 3251–3257 (1987).
- Jeon, I. Y. *et al.* Facile, scalable synthesis of edge-halogenated graphene nanoplatelets as efficient metal-free electrocatalysts for oxygen reduction reaction. *Sci. Rep.-Uk* **3** (2013).
- Chen, P., Xiao, T. Y., Qian, Y. H., Li, S. S. & Yu, S. H. A Nitrogen-Doped Graphene/Carbon Nanotube Nanocomposite with Synergistically Enhanced Electrochemical Activity. *Adv. Mater.* **25**, 3192–3196 (2013).
- Peng, H. L. *et al.* High Performance Fe- and N- Doped Carbon Catalyst with Graphene Structure for Oxygen Reduction. *Sci. Rep.-Uk* **3** (2013).
- Ohnishi, R., Takanabe, K., Katayama, M., Kubota, J. & Domen, K. Nano-nitride Cathode Catalysts of Ti, Ta, and Nb for Polymer Electrolyte Fuel Cells: Temperature-Programmed Desorption Investigation of Molecularly Adsorbed Oxygen at Low Temperature. *J. Phys. Chem. C* **117**, 496–502 (2013).
- Chen, J. *et al.* Nano-sized TiN on carbon black as an efficient electrocatalyst for the oxygen reduction reaction prepared using an mpg-C₃N₄ template. *Chem. Commun.* **46**, 7492–7494 (2010).
- Ohnishi, R. *et al.* Titanium Nitride Nanoparticle Electrocatalysts for Oxygen Reduction Reaction in Alkaline Solution. *J. Electrochem Soc.* **160**, F501–F506 (2013).
- Janes, R. A., Aldissi, M. & Kaner, R. B. Controlling Surface Area of Titanium Nitride Using Metathesis Reactions. *Chem. Mater.* **15**, 4431–4435 (2003).
- Rodríguez-Reyes, J. C. F., Ni, C., Bui, H. P., Beebe, T. P. & Teplyakov, A. V. Reversible Tuning of the Surface Chemical Reactivity of Titanium Nitride and Nitride-Carbide Diffusion Barrier Thin Films. *Chem. Mater.* **21**, 5163–5169 (2009).
- Zhang, J., Xue, Q. & Li, S. X. Microstructure and corrosion behavior of TiC/Ti(CN)/TiN multilayer CVD coatings on high strength steels. *Appl. Surf. Sci.* **280**, 626–631 (2013).
- Merki, D. & Hu, X. L. Recent developments of molybdenum and tungsten sulfides as hydrogen evolution catalysts. *Energy Environ. Sci.* **4**, 3878–3888 (2011).
- Liang, Y. Y. *et al.* Oxygen Reduction Electrocatalyst Based on Strongly Coupled Cobalt Oxide Nanocrystals and Carbon Nanotubes. *J. Am. Chem. Soc.* **134**, 15849–15857 (2012).
- Benck, J. D., Chen, Z. B., Kuritzky, L. Y., Forman, A. J. & Jaramillo, T. F. Amorphous Molybdenum Sulfide Catalysts for Electrochemical Hydrogen Production: Insights into the Origin of their Catalytic Activity. *ACS Catal.* **2**, 1916–1923 (2012).
- Bard, A. J. & Faulkner, L. R. *Electrochemical Methods: Fundamentals and Applications*. (Wiley: New York, 2001).

Acknowledgments

We thank Chengdu Tool Research Institute Co. Ltd and South Petroleum University for supplying CVD device. This work was supported by the National Nature Science Foundation of China (no. 21275104).

Author contributions

D.X. designed and conceived the experiments and Z.Y.J. carried out the characterizations of the catalyst. Z.Y.J. and P.P.L. took the electrochemical measurements and the calculations. Z.Y.J. wrote the paper and all authors contributed to discussions about the results and the manuscript.

Additional information

Supplementary information accompanies this paper at <http://www.nature.com/scientificreports>

Competing financial interests: The authors declare no competing financial interests.

How to cite this article: Jin, Z., Li, P. & Xiao, D. Enhanced Electrocatalytic Performance for Oxygen Reduction via Active Interfaces of Layer-By-Layered Titanium Nitride/Titanium Carbonitride Structures. *Sci. Rep.* **4**, 6712; DOI:10.1038/srep06712 (2014).



This work is licensed under a Creative Commons Attribution-NonCommercial-NoDerivs 4.0 International License. The images or other third party material in this article are included in the article's Creative Commons license, unless indicated otherwise in the credit line; if the material is not included under the Creative Commons license, users will need to obtain permission from the license holder in order to reproduce the material. To view a copy of this license, visit <http://creativecommons.org/licenses/by-nc-nd/4.0/>